analytical chemistry

Article

pubs.acs.org/ac

Continuous Fluorescence Assays for Reactions Involving Adenine

Ross S. Firestone,[†] Scott A. Cameron,[†] Peter C. Tyler,[‡] Rodrigo G. Ducati,[†] Adam Z. Spitz,[†] and Vern L. Schramm*[,†]

[†]Department of Biochemistry, Albert Einstein College of Medicine, 1300 Morris Park Avenue, Bronx, New York 10461, United States

[‡]The Ferrier Research Institute, Victoria University of Wellington, Lower Hutt, Wellington 6140, New Zealand

Supporting Information

ABSTRACT: 5′-Methylthioadenosine phosphorylase (MTAP) and 5′-methylthioadenosine nucleosidase (MTAN) catalyze the phosphorolysis and hydrolysis of 5′-methylthioadenosine (MTA), respectively. Both enzymes have low K_M values for their substrates. Kinetic assays for these enzymes are challenging, as the ultraviolet absorbance spectra for reactant MTA and product adenine are similar. We report a new assay using 2-amino-5′-methylthioadenosine (2AMTA) as an alternative substrate for MTAP and MTAN enzymes. Hydrolysis or phosphorolysis of 2AMTA forms 2,6-diaminopurine, a fluorescent and easily quantitated product. We kinetically characterize 2AMTA with human MTAP, bacterial MTANs and use 2,6-diaminopurine as a fluorescent substrate for yeast adenine phosphoribosyltransferase. 2AMTA was used as the substrate to kinetically characterize the dissociation constants for three-transition-state analogue inhibitors of MTAP and MTAN. Kinetic values obtained from continuous fluorescent assays with MTA were in good agreement with previously measured literature values, but gave smaller experimental errors. Chemical synthesis from ribose and 2,6-dichloropurine provided crystalline 2AMTA as the oxalate salt. Chemo-enzymatic synthesis from ribose and 2,6-diaminopurine produced 2-amino-*S*-adenosylmethionine for hydrolytic conversion to 2AMTA. Interaction of 2AMTA with human MTAP was also characterized by pre-steady-state kinetics and by analysis of the crystal structure in a complex with sulfate as a catalytically inert analogue of phosphate. This assay is suitable for inhibitor screening by detection of fluorescent product, for quantitative analysis of hits by rapid and accurate measurement of inhibition constants in continuous assays, and pre-steady-state kinetic analysis of the target enzymes.

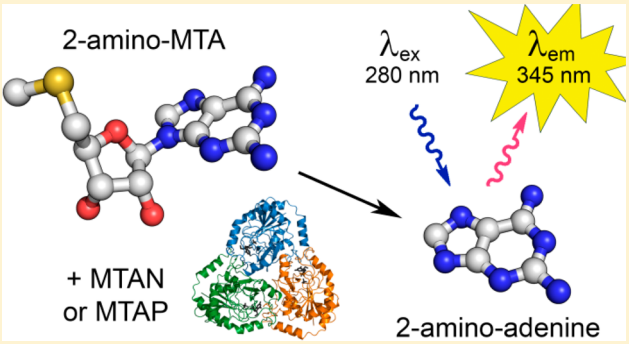

Human 5′-methylthioadenosine phosphorylase (MTAP) metabolizes 5′-methylthioadenosine (MTA) formed in the polyamine pathway, which is responsible for cellular synthesis of spermidine and spermine from putrescine.[1] Polyamine synthesis involves the donation of two *n*-propylamino groups from *S*-adenosyl-L-methioninamine (decarboxy-AdoMet) to putrescine to form spermine and two molecules of MTA as an end product metabolite.[2] The polyamine pathway is the only site of MTA formation in humans and MTAP is the only enzyme for MTA metabolism. The phosphorolysis of MTA produces adenine and methylthioribose-1-phosphate (MTR1P). Adenine is salvaged to the nucleotide pool by adenine phosphoribosyltransferase and MTR1P is a precursor for methionine. Salvage of AdoMet is completed by synthesis of AdoMet from ATP and L-methionine by *S*-adenosyl-L-methionine synthetase (MAT2A) in humans.

Most bacterial species lack MTAP. Instead, MTA is hydrolyzed by 5′-methylthioadenosine/*S*-adenosylhomocysteine nucleosidase (MTAN) through a reaction that forms adenine and methylthioribose.[3] Bacterial pathways for salvage of methylthioribose and adenine are also capable of reforming these products to *S*-adenosyl-L-methionine.[4]

Polyamine synthesis and AdoMet salvage pathways are critical for rapid cellular growth, making MTAP a target for potential anticancer therapeutics.[5−8] Deletions of the MTAP/CDKN2A region occur in approximately 15% of human cancers, and these mutations make cancer cells highly sensitive to inhibitors of the histone arginine methyltransferase, PRMT5.[9−11] This mechanism is proposed to be cellular accumulation of MTA which competes at the catalytic site of PRMT5 for AdoMet. Transition state analogues of MTAP have been reported and show anticancer effects in mouse xenograft models of human head and neck and lung cancers as a result of MTA accumulation.[12,13] Because MTAP deletion makes MTAP/CDKN2A-deleted cancers susceptible to PRMT5 inhibitors, a combination of MTAP and PRMT5 inhibitors would be of interest to explore as a mechanism to enhance PRMT5 inhibitor therapy.[9] This increased interest in MTAP/CDKN2A deletion and catalytic activity will be fostered by a

Received: September 13, 2016
Accepted: October 25, 2016
Published: October 25, 2016

DOI: 10.1021/acs.analchem.6b03621
Anal. Chem. XXXX, XXX, XXX−XXX

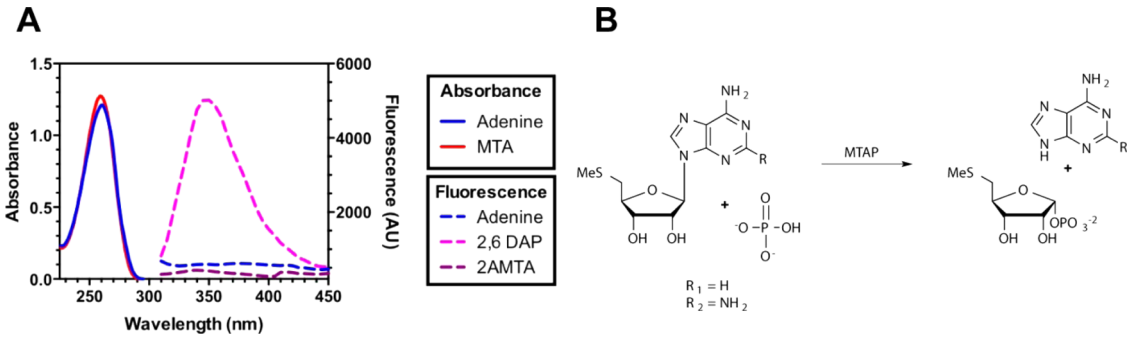

Figure 1. MTAP mediated phosphorolysis. (A) The UV absorbance spectral change for equal concentrations of MTA and adenine (solid lines) and the fluorescence emission spectra for equal concentrations of adenine, 2,6-diaminopurine and 2-amino-MTA (dashed lines). (B) The phosphorolysis of MTA catalyzed by MTAP to form adenine and 5-methylthio-α-D-ribose-1-phosphate as products. R_1 represents 5′-methylthioadenosine (MTA), the natural substrate of MTAP and R_2 represents 2-amino-5′-methylthioadenosine (2AMTA), which forms 2,6-diaminopurine, as a highly fluorescent product.

robust assay suited to high-throughput screening and quantitative analysis of inhibitor action.

Inhibitors of bacterial MTAN enzymes are of interest because the 5-methylthioribose formed by the action of MTAN is a metabolic precursor for autoinducer-2 (AI-2) quorum sensing molecules in Gram-negative bacteria.[14] Inhibition or gene deletion of bacterial MTAN causes complete inhibition of AI-2 production, a target for the expression of pathogenicity genes in disease-related bacteria.[15,16] In a few species, including *Helicobacter pylori*, MTAN activity is required for the synthesis of menaquinone, an essential electron transfer metabolite in this organism.[17,18] Transition-state analogue inhibitors of *H. pylori* MTAN are more powerful antibiotics against this organism than any of the antibiotics currently approved for *H. pylori* infections.[19,20]

The K_M values for MTA with some of the bacterial MTAN enzymes are in the low nM range, making kinetic analysis difficult from the low inherent ultraviolet spectral change on conversion of MTA to adenine and 5-methylthioribose. The more sensitive fluorescent assay described here will augment the investigation of bacterial MTANs, human MTAP and adenine phosphoribosyltransferase.

Transition-state analysis of human MTAP and several bacterial MTANs has led to the design of transition-state analogues that are high affinity, competitive inhibitors at the catalytic sites of both MTAP and MTANs with dissociation constants in the picomolar range.[21,22] A crucial step in developing and evaluating transition-state analogues is the measurement of inhibition constants (K_i) through assessment of enzyme activity in the presence of potential inhibitors. Current methods to monitor MTAP and MTAN activity are limited, and often coupled to one or more accessory enzymes to convert adenine to chromophores with higher signal output. Direct measurement of absorbance change following the conversion of MTA to adenine is not effective because of the small difference in UV absorbance between the two compounds (Figure 1A). Coupling enzymes including xanthine oxidase[23] and firefly luciferase[24] have been used to generate more easily quantified products, but coupled assays are necessarily inferior to direct assays, as coupling enzymes add a lag in reaction rate and may also be inhibited by the compounds being tested. MTAP and MTAN enzyme activities can also be quantitated by radiolabeled substrates with analysis of product quantities following HPLC purification or other separation method. These discontinuous assays are slow, expensive, and not easily scaled for detailed kinetic analyses or high-throughput assays.

We developed a new assay using 2-amino-5′-methylthioadenosine (2AMTA) as an alternative substrate for measuring MTAP and MTAN catalytic activity. Loss of the *N*-ribosyl bond of 2AMTA produces 2,6-diaminopurine, easily quantified through fluorescence measurement (Figure 1). We have defined two synthetic paths for production of 2AMTA and have characterized the kinetics of MTAP, MTAN and adenine phosphoribosyltransferase reactions using 2AMTA as substrate. This substrate can be used to accurately measure the K_i values for inhibitors of adenine forming enzymes by direct assays, without the use of coupling enzymes or discontinuous assays.

MATERIALS AND METHODS

Preparation of MTAP and MTAN Enzymes. MTAP and MTAN enzymes were prepared as previously described.[28,34] Co-purified active site adenine was removed via dialysis of purified protein against 100 mM potassium phosphate with 1 mM DTT and 1.5 g/L activated charcoal at a pH = 7.4 overnight. The adenine-free enzymes were then dialyzed against the same buffer without the activated charcoal and concentrated to 250 μM stock solutions. Enzymes were stored at −80 °C in the dialysis buffer.

Chemoenzymatic Synthesis of 2AMTA. 2-Amino-ATP was synthesized in a 1 mL solution containing 2 mM D-ribose, 2 mM 2,6-diaminopurine, 20 μM ATP, 20 mM phosphoenolpyruvic acid, 6 mM ammonium chloride, 5 mM magnesium chloride, 50 mM potassium chloride and 100 mM potassium phosphate (Figure 2). The solution was buffered to pH = 8.0 before adding 1 unit each of ribokinase, adenine phosphoribosyltransferase (APRTase), 5′-phosphoribosylpyrophosphate synthetase (PRPPase), adenylate kinase, and pyruvate kinase to initiate the reaction. Adenylate kinase and pyruvate kinase were purchased from Sigma-Aldrich, while ribokinase, PRPPase, and APRTase were expressed in *E. coli* and used as previously described.[25] The reaction was incubated at room temperature overnight, and was quenched by the addition of 110 mL of 0.1 M sulfuric acid to give a final concentration 0.01 M. The resulting 2-amino-ATP was purified from other reaction contents by reverse phase HPLC using a Kinetex C18 250 mm × 4.6 mm column eluted with 50 mM potassium phosphate and 8 mM tetrabutylammonium bisulfate (pH = 6.0), as previously described.[35] 2AMTA was prepared in a 1 mL solution containing 1 mM 2-amino-ATP, 8 mM L-methionine,

DOI: 10.1021/acs.analchem.6b03621
Anal. Chem. XXXX, XXX, XXX−XXX

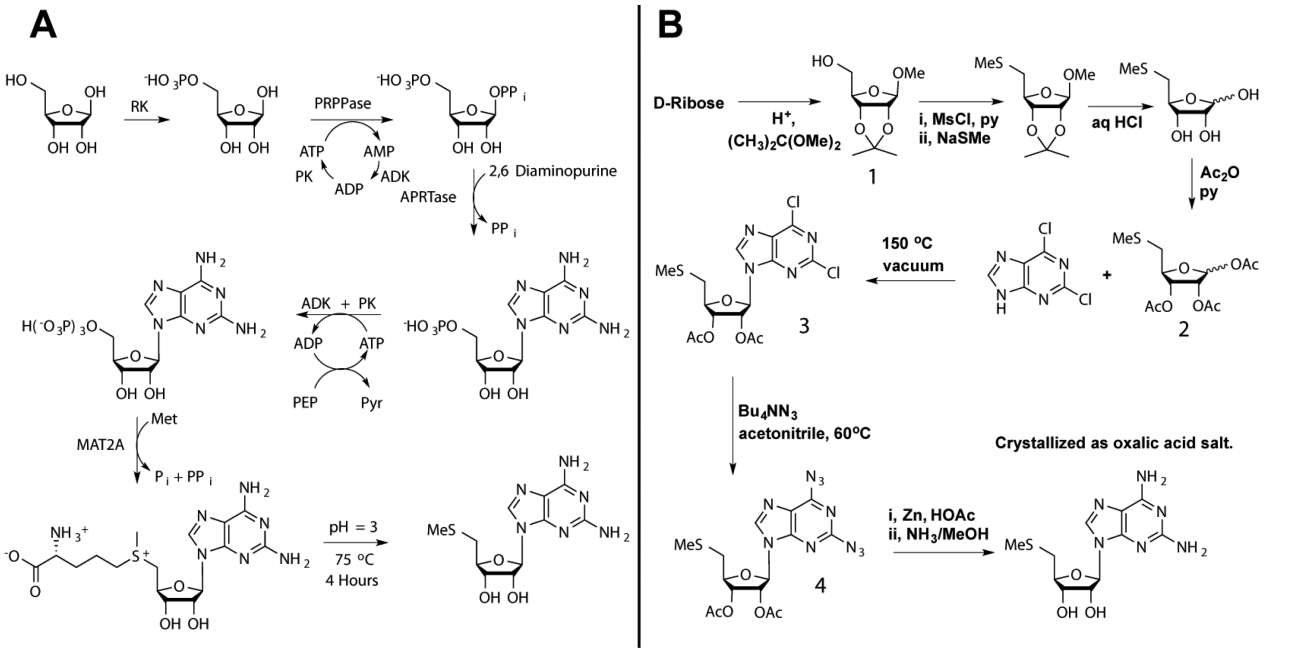

Figure 2. Synthetic schemes for 2AMTA. (A) Chemoenzymatic and (B) chemical synthesis procedures for production of 2AMTA. Both syntheses use D-ribose as starting material. In panel A, abbreviations are for ribokinase (RK), phosphoribosyl pyrophosphate synthetase (PRPPase), adenine phosphoribosyltransferase (APRTase), adenylate kinase (ADK), pyruvate kinase (PK), methionine adenosyltransferase (MAT2A), phosphoenolpyruvic acid (PEP), and pyruvate (Pyr). The yield of 2AMTA from ribose as limiting reagent in A was 85%. In B, the overall yield from ribose was 14%.

50 mM tris-HCl, 50 mM potassium chloride, and 10 mM magnesium chloride. The solution was buffered to pH = 9.0 with potassium hydroxide before initiating the reaction with 2 μM human methionine adenosyltransferase (MAT2A).[36] The reaction was incubated at room temperature for 4 h and was then brought to pH = 3.0 with 6 M H_2SO_4 and incubated at 75 °C overnight. The 2AMTA product was purified from other reaction contents with the reverse phase HPLC protocol described above..

Chemical Synthesis of 2AMTA. A mixture of **1** (See Figure 2B) (8.24 g, 35.2 mmol), dioxane (20 mL), water (75 mL) and concentrated HCl (1.5 mL) was heated at 80 °C for 1h, concentrated to dryness, redissolved in pyridine and evaporated. The residue was treated with pyridine (30 mL) and acetic anhydride (30 mL) and the solution stirred at room temperature for 16 h before being evaporated and coevaporated with toluene (×4). Chromatography of the residue afforded the syrupy triacetate **2** (5.21 g, 17 mmol, 48%) as an anomeric mixture. A mixture of **2** (4.10 g, 13.4 mmol) and 2,6-dichloropurine (3.29 g, 17.4 mmol) was heated with stirring at 150 °C under vacuum. After 1 h the dark oil was cooled, dissolved in chloroform, and the solution was washed with aqueous $NaHCO_3$, dried and concentrated. Chromatography of the residue afforded syrupy **3** (4.10 g, 9.42 mmol, 70%) as an anomeric mixture. A solution of this material (2.13 g, 4.89 mmol) and tetrabutylammonium azide (5.57 g, 19.6 mmol) in acetonitrile (40 mL) was heated at 60 °C for 4 h and then concentrated to dryness. The residue was dissolved in chloroform and the solution was washed with water (×2), dried and concentrated. Chromatography of the residue (20–50% ethyl acetate/petroleum ether) afforded syrupy **4** (0.924 g, 2.06 mmol, 42%) free from its alpha anomer.[1]H NMR (500 MHz, $CDCl_3$) δ 8.14 (s, 1H), 6.12 (d, J = 5.4 Hz, 1H), 5.89 (t, J = 5.6 Hz, 1H), 5.57 (dd, J = 5.8, 4.7 Hz, 1H), 4.49–4.37 (m, 1H), 3.03–2.89 (m, 2H), 2.16 (s, 3H), 2.15 (s, 3H), 2.07 (s, 3H). Zinc powder (2.34 g, 35.8 mmol) was added to a solution of **4** (0.802 g, 1.79 mmol) in acetic acid (25 mL) and the mixture was stirred at RT for 2.5 h and then filtered, the solids washed with HOAc and the filtrate was concentrated to dryness. The residue in chloroform was washed with aqueous $NaHCO_3$, dried and concentrated. Chromatography (0–10% MeOH/EtOAc), gave a foam (0.484 g, 1.2 mmol, 68%). This material (0.43 g, 1.085 mmol) was dissolved in 7 N ammonia in methanol (30 mL), and after 2 h was concentrated to dryness. The residue was dissolved in water and evaporated, then redissolved in water and oxalic acid (0.0987 g, 1.085 mmol) was added. Evaporation gave a white solid which was triturated with acetone and filtered affording 2AMTA oxalic acid salt (0.348 g, 0.87 mmol, 80%). [1]H NMR (500 MHz, D_2O) δ 8.09 (s, 1H), 5.86 (d, J = 5.2 Hz, 1H), 4.78 (t, J = 5.2 Hz, 1H), 4.36 (t, J = 4.9 Hz, 1H), 4.26 (dt, J = 6.9, 4.8 Hz, 1H), 2.98–2.83 (m, 2H), 2.09 (s, 3H). [13]C NMR (126 MHz, D_2O) δ 165.73, 152.39, 151.60, 149.91, 140.35, 111.60, 87.65, 83.38, 73.19, 72.43, 35.83, 15.19. HRMS calcd for MH+ $C_{11}H_{17}N_6O_3S$, 313.1083; Found, 313.1085.

Kinetic Characterization of 2AMTA with MTAP and MTAN. Three enzymes were initially tested to determine if 2AMTA was a viable alternative substrate. Human MTAP and *Helicobacter pylori* MTAN were both able to use 2AMTA as a substrate however no reaction was observed in the case of *Escherichia coli* MTAN. Michaelis constants for 2AMTA were determined in solutions of 100 mM potassium phosphate (pH = 7.4) and 1 mM DTT with varying concentrations of 2AMTA. Appropriate amounts of enzyme (5 nM of *hp*MTAN monomer or 50 nM of *hs*MTAP monomer) were added to reaction mixtures of 200 μL under ambient conditions in a Greiner Bio One 96-Well Cellstar microplate. Product formation was monitored by an excitation wavelength of 280 nm and an

DOI: 10.1021/acs.analchem.6b03621
Anal. Chem. XXXX, XXX, XXX–XXX

emission wavelength of 345 nm using an M5 spectramax microplate reader. Assays were run for 2 h and reactions were not terminated chemically. Resulting data was fit to the Michaelis−Menten equation to determine Michaelis constants (Figure 4, eq 1).

In screening bacterial MTANs to determine 2AMTA specificity, 200 μL reactions were prepared containing 100 mM potassium phosphate (pH = 7.4) with 1 mM DTT, 1 mM 2AMTA, and 1 μM of the respective enzyme. The rate of product formation was determined using the same method as above. For those MTANs not active with 2AMTA, all were confirmed to be active in assays for MTA conversion to adenine using the assay coupled to xanthine oxidase.

$$v_0 = \frac{V_{max}[S]}{K_m + [S]} \quad (1)$$

Kinetic Characterization of *Saccharomyces cerevisiae* Adenine Phosphoribosyltransferase. *Saccharomyces cerevisiae* adenine phosphoribosyltransferase (*sc*APRTase) was purified as previously described.[42] The Michaelis constant for 2,6-diaminopurine was determined in 250 μL reactions containing 50 mM Tris HCl, 5 mM $MgCl_2$, 8 mg/mL BSA, 1 mM PRPP, and varying concentrations of 2,6-diaminopurine. The reaction was initiated by adding 100 nM of *sc*APRTase and the decrease in 2,6-diaminopurine concentration was measured using the fluorescence signal as described above. Data was fit to eq 1.

Inhibition Constants for MTAP/MTAN Inhibitors. Three transition-state analogues of MTAP and MTAN, Methylthio-Immucillin-A (MT-ImmA), Methylthio-DADMe-Immucillin-A (MT-DADMe-ImmA) and *p*Cl-PhT-DADMe-Immucillin-A (pCl-PhT-DADMe-ImmA), have been reported as powerful inhibitors of these enzymes with K_i^* values in the nM to pM range.[20−22] The K_i^* values of these three inhibitors were determined with the 2AMTA fluorescence-based assay to compare with literature values. K_i^* values were measured in solutions containing 100 mM potassium phosphate, 1 mM DTT, and 1−3 mM 2AMTA with varying concentrations of inhibitor. The rate of formation of the fluorescent 2,6-diaminopurine product was measured over time and the resulting data was fit to the Morrison quadratic equation to account for inhibitor depletion by the inhibited enzyme complex (Figure 4, eq 2).[30]

$$v = v_0\left(1 - \left([E_T] + [I] + \left(K_i\left(1 + \frac{[S]}{K_m}\right)\right)\right) - \frac{\sqrt{\left([E_T] + [I] + K_i\left(1 + \frac{[S]}{K_m}\right)\right)^2 - 4[E_T][I]}}{2[E_T]}\right) \quad (2)$$

MTAP Pre-Steady-State Kinetics. Presteady-state kinetics experiments for the MTAP-catalyzed phosphorolysis of 2AMTA were conducted on an Applied Photophysics model SX20 stopped-flow instrument, which has a dead time near 1 ms. Each experiment was an average of at least 12 measurements under identical conditions. The reaction was monitored by measuring the change in fluorescence at 345 nm given an incident light at 280 nm. Measurements were taken by mixing 60 μL quantities of 10 μM MTAP in 100 mM potassium phosphate and 1 mM DTT together with a substrate solution containing varying concentrations of 2AMTA in the same buffer (Figure 5). The resulting data was fit to an exponential-linear function (eq 3) where Y is the measured fluorescence, A is the signal amplitude, K is the rate of the exponential phase, ν is the rate of the linear phase, c is the initial fluorescence value and x is time.

$$Y = A \times e^{(-Kx)} + \nu x + c \quad (3)$$

The ratio of fluorescence signal to product concentration was also measured in the stopped-flow instrument by mixing known concentrations of 2,6-DAP and fitting the resulting fluorescence standard curve to a linear regression. The off-rate (k_{off}) for 2,6-DAP product was determined by injecting 60 μL of a solution of 3 μM MTAP with excess 2,6-DAP into a 60 μL solution of sample buffer and observing the decrease in 2,6 DAP fluorescence intensity following the 2-fold dilution. The data was fit to a first-order rate equation to determine an apparent k_{off} rate for 2,6-DAP.

Crystallization of *hs*MTAP with 2AMTA and Sulfate. Charcoal-purified *hs*MTAP was dialyzed against 100 mM sulfate and 1 mM DTT at a pH = 8.0, concentrated to 15 mg/mL and incubated with 5 equiv of 2AMTA. The protein was crystallized with the *N*-terminal TEV cleavage site and His_6 tag intact at 22 °C using the sitting drop vapor-diffusion technique. Hexagonal rod-shaped crystals (100 μm × 100 μm × 250 μm) were obtained overnight using 0.2 M magnesium chloride and 20% (w/v) polyethylene glycol 3350.

The ligand-bound *hs*MTAP crystals were transferred to a cryoprotectant solution containing 20% (v/v) glycerol and the mother liquor [80% (v/v)] prior to being flash-cooled in liquid nitrogen. Diffraction data for *hs*MTAP·2-amino-MTA crystals were collected with 0.9793 Å wavelength radiation at the LRL-CAT beamline (Argonne National Laboratory, Argonne, IL) on a Rayonix 225 HE CCD detector to 1.80 Å resolution. Diffraction intensities were integrated and scaled with Denzo and Scalepack.[37] The diffraction data statistics are summarized in Table 1.

The structure of *hs*MTAP·2AMTA was determined by molecular replacement with Molrep,[38] using a single monomer from the previously published structures of *hs*MTAP·MeS-Immucillin-A (PDB entry 1K27) as a search model.[33] The refinement of the initial solution and subsequent refinements were conducted using a restrained refinement performed with Refmac,[39] using all data between 25.0 and 1.80 Å. Manual model rebuilding was conducted using Coot.[40] Difference Fourier maps calculated with $F_{obs} - F_{calc}$ coefficients revealed ordered water and sulfate molecules and strong unambiguous density difference, corresponding to the 2AMTA substrate. The mmCIF component definition file for this substrate was created using JLigand.[41] Water molecules with proper hydrogen bonding coordination and electron densities greater than one rmsd and three rsmds in maps calculated with $2F_{obs} - F_{calc}$ and $F_{obs} - F_{calc}$ coefficients, respectively, were included in the model. Residues 10−281 of the HsMTAP sequence were sufficiently ordered to be included in the model. None of the 14 residues in the cleavage/His6 tag were included in the model. This structure was refined to an R_{cryst} of 16.9% and an R_{free} of 19.3%. Analysis of the structures in Coot revealed good stereochemistry with no residues falling into the disallowed region of the Ramachandran plot. The refinement statistics are listed in Table 1.

DOI: 10.1021/acs.analchem.6b03621
Anal. Chem. XXXX, XXX, XXX−XXX

Table 1. Data Collection and Refinement Statistics

data collection	
space group	*P*321
no. of molecules in the asymmetric unit	1
cell dimensions	
a, *b*, *c* (Å)	121.504, 121.504, 45.328
resolution (Å)[a]	50.0−1.80 (1.83−1.80)
no. of unique reflections[a]	35008 (1719)
R_{merge}[a]	0.091 (0.738)
$I/\sigma I$[a]	23.4 (2.8)
completeness (%)[a]	98.7 (99.8)
refinement	
resolution (Å)	25.0−1.80
R_{cryst}	0.169
R_{free}	0.193
rmsd	
bond lengths (Å)	0.009
bond angles (deg)	1.46
no. of atoms (average *B* factor)	
proteins	2083 (25.9)
substrate	21 (23.0)
waters	180 (33.6)
phosphates	10 (38.4)
other	13 (41.9)
PDB entry	5EUB

[a]Numbers in parentheses indicate values for the highest-resolution shell.

RESULTS AND DISCUSSION

Synthesis of 2AMTA. Chemoenzymatic and chemical synthetic schemes were developed for the production of 2AMTA. The chemoenzymatic method is based on a previous reported synthesis of AMP[25] except for substitution of adenine by 2,6-diaminopurine in the APRTase catalyzed step (Figure 2A). This synthetic approach relies on the enzymatic promiscuity of APRTase, adenylate kinase and pyruvate kinase to accept 2,6-diaminopurine and 2,6-diaminopurine nucleotides as substrates. All three enzymes were able to catalyze their respective reactions with these 2,6-diaminopurine-containing substrates without prohibitive reductions in reaction rate. The chemical synthesis was based on a modified literature synthesis and the product was crystallized in the form of an oxalic acid salt (Figure 2B).[26,27]

Kinetic Characterization of 2AMTA with MTAP and MTAN. Use of 2AMTA as an alternative substrate for fluorescence-based kinetic assays is dependent on the enzymatic promiscuity of MTA cleavage enzymes. We initially tested human MTAP, *Helicobacter pylori* MTAN and *Escherichia coli* MTAN to determine if 2AMTA was a viable alternative substrate. Phosphorolysis of 2AMTA to MTR1P and 2,6-diaminopurine was observed for human MTAP and hydrolysis of 2AMTA to 2,6-diaminopurine was observed with *Helicobacter pylori* MTAN. In contrast, the *Escherichia coli* isoform of MTAN was inactive with 2AMTA, showing greater than a thousand-fold reduction in rate compared to *hp*MTAN. In addition, 2AMTA did not act as an inhibitor with respect to MTA at concentrations up to 300 μM, consistent with a low catalytic site affinity.

Human MTAP and *H. pylori* MTAN catalytic activity on 2AMTA was monitored at multiple concentrations of substrate to determine the Michaelis constants (K_M) and turnover numbers (k_{cat}) for each enzyme (Table 2, Figure 4, eq 1). The catalytic efficiency (k_{cat}/K_M) for both enzymes decreased by approximately a factor of 10 with 2AMTA relative to MTA. However, this difference results primarily from an increased K_M value for 2AMTA, suggesting decreased affinity of 2AMTA with only modest changes in catalytic cycling (k_{cat}) for these enzymes.

The utility of the 2AMTA assay for MTANs was tested with enzymes from six additional bacterial species. MTANs from *Neisseria meningitidis*, *Salmonella enterica*, *Yersinia pestis*, and *Staphylococcus aureus* catalyzed the hydrolysis of the 2AMTA nucleosidic bond. However, MTANs from *Streptococcus pneumoniae* and *Vibrio chlorae* were unable to hydrolyze 2AMTA at significant rates at an enzyme concentration of 1 μM and a substrate concentration of 1 mM (see Table 3). While 2AMTA provides a useful alternative substrate for five of the eight MTANs tested, not all species of MTAN can be studied with this assay.

Table 3. Kinetic Constants for Bacterial MTANs with the 2AMTA Assay

MTAN species	K_M (μM)	k_{cat} (s^{-1})	k_{cat}/K_M (10^5 M)
Neisseria meningitidis	7 ± 1.9	1.9 ± 0.27	2.7 ± 1.2
Salmonella enterica	8 ± 1.6	1.6 ± 0.18	2.0 ± 0.64
Yersinia pestis	11 ± 4.4	1.1 ± 0.28	1.0 ± 0.66
Staphylococcus aureus	10.4 ± 4.2	1.8 ± 0.26	1.7 ± 0.77
Streptococcus pneumoniae	N/A	$<10^{-5}$	N/A
Vibrio cholerae	N/A	$<10^{-5}$	N/A

Analysis of the structures and sequences of the MTANs studied was carried out (see Supporting Information). Notably, *S. enterica* and *E. coli* MTANs are 96% identical by sequence, with only nine residues different (mostly conservative changes). All of these residues are at or near the protein surface and are distal to the active site. Yet surprisingly, the former MTAN is active with regards to 2AMTA hydrolysis, whereas the latter is not. From inspection of structure or sequence alone, the

Table 2. Kinetic Constants for MTA and 2AMTA with *hs*MTAP and *hp* or *ec*MTANs.[a]

	MTA			2AMTA		
enzyme	k_{cat} (s^{-1})	K_M (μM)	k_{cat}/K_M (10^5 $M^{-1}s^{-1}$)	k_{cat} (s^{-1})	K_M (μM)	k_{cat}/K_M (10^5 $M^{-1}s^{-1}$)
*hs*MTAP	2.5 ± 0.7	5.0 ± 1.0	5 ± 1.7	1.7 ± 0.2	34 ± 7	0.50 ± 0.06
*hp*MTAN[b]	12.1 ± 2.3	0.6 ± 0.3	200 ± 110	7.0 ± 0.4	3.1 ± 0.5	23 ± 4
*ec*MTAN[b]	2.3 ± 0.1	0.19 ± 0.02	121 ± 5	N/A[c]	N/A[c]	N/A[c]

[a]Values for K_M, k_{cat}, and k_{cat}/K_M for MTAP/MTAN-mediated 2AMTA activity are from the data in Figure 4. Human (*hs*), *Helicobacter pylori* (*hp*) and *E. coli* (*ec*) enzymes are compared. No activity (N/A) was observed for *ec*MTAN under conditions that would have detected 10^{-3} the signal observed for MTA under the same conditions for *H. pylori* MTAN [b]k_{cat} and K_M values for *hp*MTAN, *ec*MTAN, and *hs*MTAP were taken from literature values.[20,28,29] [c]No activity could be detected under conditions sensitive to 10−5 of the k_{cat}/K_M with *hp*MTAN.

DOI: 10.1021/acs.analchem.6b03621
Anal. Chem. XXXX, XXX, XXX−XXX

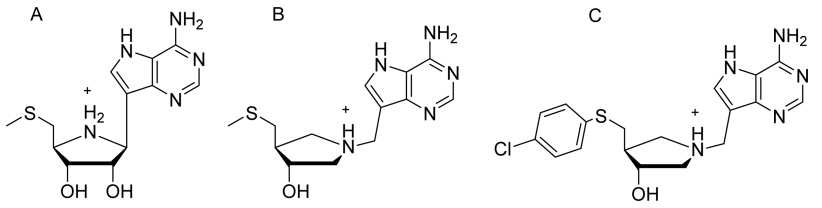

Figure 3. MTAP and MTAN Inhibitor Structures. (A) MT-ImmA, (B) MT-DADMe-ImmA, (C) *p*Cl-PhT-DADMe-ImmA.

Table 4. Inhibition of MTAP/MTAN with Transition State Analogue Inhibitors[a]

	MT-ImmA K_i^*		MT-DADMe-ImmA K_i^*		pCl-PhT-DADMe-ImmA K_i^*	
enzyme	measured	literature	measured	literature	measured	literature
*hs*MTAP	330 ± 68 pM	1 ± 0.5 nM	63 ± 10 pM	90 ± 10 pM	47 ± 13 pM	10 ± 5 pM
*hp*MTAN	66 ± 11 pM	40 ± 20 pM	15 ± 1.4 pM	89 ± 19 pM	360 ± 32 pM	570 ± 90 pM

[a]The K_i^* values of three transition state analogues were measured (Figures 3 and 4) and compared to literature values. Most values are similar to previously reported values, but show a smaller margin of error.[21,22]

differences in activity would be difficult, if not impossible, to predict. It is likely that the dynamic properties of MTANs have an important role in the apparent 2AMTA hydrolysis activity.

Kinetic Characterization of *Saccharomyces cerevisiae* Adenine Phosphoribosyltransferase. *Saccharomyces cerevisiae* adenine phosphoribosyltransferase (*sc*APRTase) was able to utilize 2,6-diaminopurine as an alternative substrate (e.g., Figure 2A). Kinetic assays of APRTases brings the same set of challenges observed for MTAP and MTAN, as adenine and AMP have small differences in absorbance spectra. We characterized the kinetics of *sc*APRTase using 2,6-diaminopurine as an alternative substrate to find the k_{cat}/K_M for 2,6-diaminopurine reduced by a factor of 800 compared to adenine with approximately 2-fold increased K_M and 400-fold decreased k_{cat} (see Figure S1, Table S1). This assay is useful for characterization of APRTase catalysis or inhibitor analysis. It should be noted that this assay involves detecting a decrease in sample fluorescence as the concentration of 2,6-diaminopurine is decreasing, rather than increasing as in the MTAP/MTAN assay. While this results in a slight decrease in the assay's signal-to-noise ratio, the assay still provides a highly sensitive method of measuring APRTase kinetics.

Determining Inhibition Constants for MTAP and MTAN Inhibitors. Use of 2AMTA as a substrate facilitated determination of K_i^* values (equilibrium dissociation constants following slow-onset inhibition) for inhibitors of MTAP and MTAN. Three previously characterized transition state analogue inhibitors, MT-ImmA, MT-DADMe-ImmA and *p*Cl-PhT-DADMe-ImmA were analyzed in slow-onset, tight-binding inhibition experiments and compared to previous reports (Figure 3).[20−22] The resulting data was fit to the Morrison equation for slow-onset, tight-binding inhibitors (Table 4, Figure 4, eq 2).[30] The dissociation constants for inhibitors determined with 2AMTA as substrate for *hp*MTAN were consistent with previously reported values, but provided a more favorable margin of experimental errors (Table 4). Previous assays depended on the uv detection of 2,8-dihydroxyadenine in a coupled assay where adenine is oxidized with xanthine oxidase.[21,22]

Disadvantages of the 2AMTA assay are (1) the reduction in catalytic efficiency observed in the APRT, MTAP and MTAN reactions of 2AMTA relative to MTA or adenine, and (2) the specificity of the *ec*MTAN, *sp*MTAN, and *vc*MTAN which did not accommodate 2AMTA as a significant substrate. Reduction

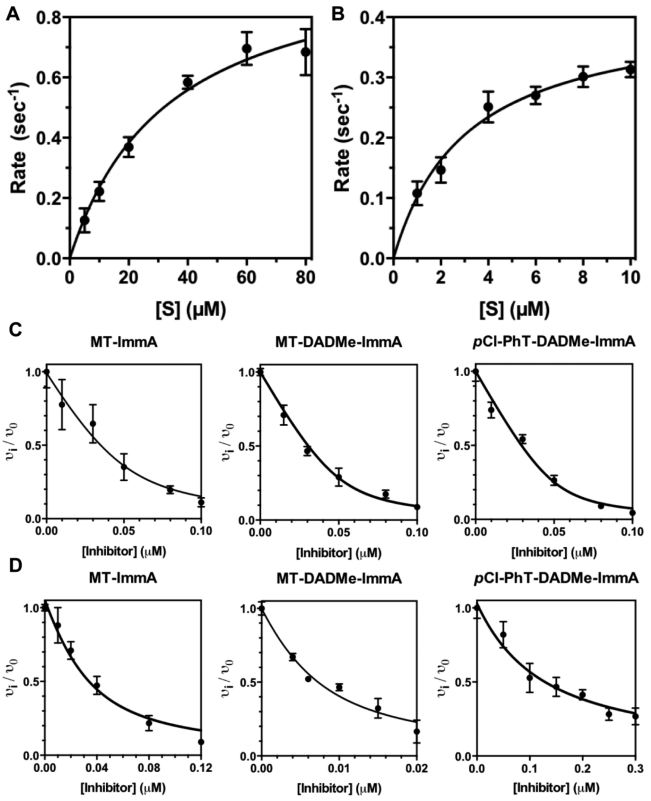

Figure 4. Kinetics of the 2AMTA assay with MTAP and MTAN. Kinetic data for the MTAP/MTAN-mediated reactions were fit to eqs 1 and 2. The Michaelis constants for (A) *hs*MTAP and (B) *hp*MTAN were determined (see Table 2). Inhibition constants for three transition-state analogue inhibitors of (C) *hs*MTAP and (D) *hp*MTAN were determined to give the kinetic constants in Table 4. Error bars report standard deviation of replicate values.

in catalytic efficiency is more than compensated by the strong fluorescent spectral signal. However, the value of 2AMTA as a kinetic probe is enzyme-dependent. The relative efficiency of *hp*MTAN, *hs*MTAP, and many bacterial MTANs with 2AMTA makes them excellent candidates for kinetic exploration using this substrate.

MTAP Pre-Steady-State Kinetics. The limited absorbance change following conversion of MTA to adenine by MTAP or MTAN is an acute problem in the presteady-state rapid

DOI: 10.1021/acs.analchem.6b03621
Anal. Chem. XXXX, XXX, XXX−XXX

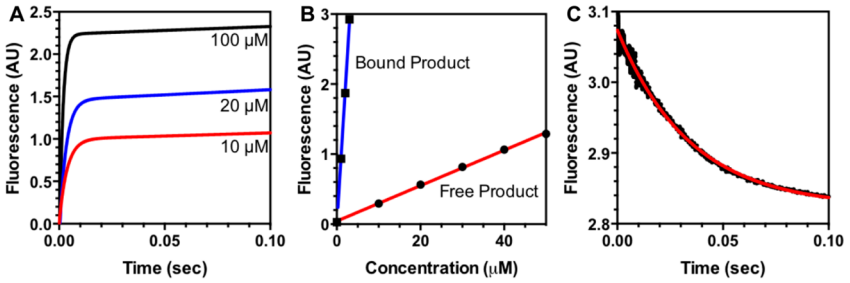

Figure 5. Pre-steady-state kinetics for MTAP phosphorolysis of 2AMTA. (A) Pre-steady-state kinetics for MTAP-mediated 2AMTA phosphorolysis were measured using stopped-flow kinetics experiments at 5 μM MTAP and varied MTA concentrations as indicated in the graph. Burst size and stead-state rate of 2AMTA increases with substrate concentration and shows a steady-state rate limited by product release. (B) The fluorescence signal from enzyme-bound 2,6-DAP exceeds the fluorescence signal from free product by 38-fold. (C) The off-rate for 2,6-DAP release is observed by the decrease in bound 2,6-DAP fluorescence intensity as it is released from the enzyme active site. The red line is the fit to a first-order process.

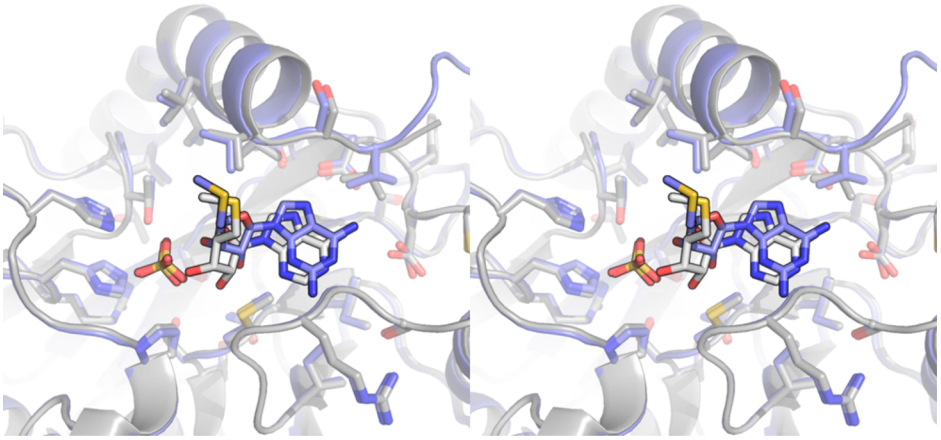

Figure 6. Crystal structure of *hs*MTAP complexed to 2AMTA and sulfate. A stereoview structural comparison of the active sites of *hs*MTAP complexed to 2AMTA (blue) and sulfate to the MTA and sulfate bound structure (white, PDB ID 1CB0). The additional 2-amino functional group lies in a hydrophobic pocket that is vacant with MTA bound at the catalytic site. No significant changes in active site structure are observed across the two structures.

reaction kinetic analysis for these enzymes. Coupled enzyme systems are not generally applicable to pre-steady-state and single-turnover kinetic studies. The pre-steady-state rate of 2AMTA phosphorolysis by *hs*MTAP was measured in stopped-flow experiments to explore the utility of 2AMTA in rapid reaction kinetics. Pre-steady-state kinetics were measured as a function of 2AMTA concentration at an enzyme concentration of 5 μM to establish the turnover numbers. An apparent turnover rate of 270 $\pm$ 1 s^{-1} was achieved at 10 μM 2AMTA (Figure 5A). Excitation of the 2,6-diaminopurine product is at 280 nm, thus the initial signal also contains a fluorescence signal from MTAP aromatic residues. A large fluorescence differential was observed (Figure 5B) with bound 2,6-DAP having a 38-fold increase in emission intensity relative to free 2,6-DAP, indicating solvent quenching for free 2,6-DAP fluorescence. This finding is reminiscent of the strong fluorescence of guanine bound to human purine nucleoside phosphorylase, but not in solution.[31,32] Additionally we determined the quantum yield of free 2,6-DAP and MTAP bound 2,6-DAP to be 0.015 $\pm$ 0.001 and 0.57 $\pm$ 0.04, respectively, through comparison to quinine fluorescence. MTAP fluorescence with MTA as a substrate was used to correct the protein contribution to fluorescence.

Pre-steady-state kinetics established a catalytic burst with fast chemistry followed by a slower steady-state rate of product release. The rate of product release (k_{off}) was also experimentally accessible by diluting a solution of MTAP-bound 2,6-DAP and observing the decrease in fluorescence signal resulting from dissociation of enzyme bound 2,6-DAP into free 2,6-DAP (Figure 5C). This off-rate was determined to be 29 $\pm$ 1 s^{-1}, which is approximately 10-fold slower than the rate of chemistry at the catalytic site with 10 μM substrate, also indicating that product release is rate limiting in the context of the steady-state reaction. The affinity of MTAP for adenine has also been recognized from the observation that MTAP is copurified from *E. coli* cell extracts with tightly bound adenine.

Crystal Structure of *hs*MTAP with Bound 2AMTA. The geometry of 2AMTA at the catalytic site of *hs*MTAP was explored by solving the crystal structure of *hs*MTAP bound to 2AMTA with sulfate as a catalytically inert substitute for phosphate. The crystal structure reveals that the 2-amino group resides in a hydrophobic pocket previously vacant in the structure of MTAP-MTA-sulfate.[33] When compared to *hs*MTAP bound to MTA, the active site structure is found to be mostly unchanged (Figure 6).

CONCLUSIONS

This work provides increased utility and sensitivity for enzymes that form or use 2,6-diaminopurine as alternative substrates. In addition, methyltransferases using 2-amino-AdoMet will form 2-amino-*S*-adenosylhomocysteine as product, readily converted to the 2,6-diaminopurine by the MTAN enzymes described here.

DOI: 10.1021/acs.analchem.6b03621
Anal. Chem. XXXX, XXX, XXX−XXX

■ ASSOCIATED CONTENT

Supporting Information

The Supporting Information is available free of charge on the ACS Publications website at DOI: 10.1021/acs.analchem.6b03621.

Kinetic characterization of 2AMTA with MTAP and MTAN, kinetic constants for *sc*APRTase, kinetics of the 2,6-diaminopurine assay, 2AMTA screen for multiple MTAN species, and sequence alignment of MTANs (PDF)

■ AUTHOR INFORMATION

Corresponding Author

*E-mail: vern.schramm@einstein.yu.edu. Phone: 718-430-2813.

Notes

The authors declare no competing financial interest.

■ ACKNOWLEDGMENTS

This work was supported by research grant R01 CA135405 and training grant T32 GM007288 from the National Institutes of Health. This research also used resources of the Advanced Photon Source, a U.S. Department of Energy (DOE) Office of Science User Facility operated for the DOE Office of Science by Argonne National Laboratory under Contract No. DE-AC02-06CH11357. Use of the Lilly Research Laboratories Collaborative Access Team (LRL-CAT) beamline at Sector 31 of the Advanced Photon Source was provided by Eli Lilly Company, which operates the facility. We thank Dr. Zhen Wang for her expert help with stopped-flow analysis.

■ REFERENCES

(1) Battaglia, V.; DeStefano Shields, C.; Murray-Stewart, T.; Casero, R. A. *Amino Acids* **2014**, *46*, 511−519.

(2) Tabor, C. W.; Tabor, H. *Annu. Rev. Biochem.* **1984**, *53*, 749−790.

(3) Parveen, N.; Cornell, K. A. *Mol. Microbiol.* **2011**, *79*, 7−20.

(4) Sekowska, A.; Denervaud, V.; Ashida, H.; Michoud, K.; Haas, D.; Yokota, A.; Danchin, A. *BMC Microbiol.* **2004**, *4*, 9.

(5) Wallace, H. M.; Fraser, A. V.; Hughes, A. *Biochem. J.* **2003**, *376*, 1−14.

(6) Bistulfi, G.; Affronti, H. C.; Foster, B. A.; Karasik, E.; Gillard, B.; Morrison, C.; Mohler, J.; Phillips, J. G.; Smiraglia, D. J. *Oncotarget* **2016**, *7*, 14380−14393.

(7) Kamatani, N.; Nelson-Rees, W. A.; Carson, D. A. *Proc. Natl. Acad. Sci. U. S. A.* **1981**, *78*, 1219−1223.

(8) Bertino, J.; Waud, W.; Parker, W.; Lubin, M. *Cancer Biol. Ther.* **2011**, *11*, 627−632.

(9) Marjon, K.; Cameron, M.; Quang, P.; Clasquin, M.; Mandley, E.; Kunii, K.; McVay, M.; Choe, S.; Kernytsky, A.; Gross, S.; Konteatis, Z.; Murtie, J.; Blake, M.; Travins, J.; Dorsch, M.; Biller, S.; Marks, K. *Cell Rep.* **2016**, *15*, 574−587.

(10) Mavrakis, K. J.; McDonald, E. R.; Billy, E.; Hoffman, G. R.; deWeck, A.; Ruddy, D. A.; Venkatesan, K.; Yu, J.; McAllister, G.; Stump, M.; deBeaumont, R.; Ho, S.; Yue, Y.; Liu, Y.; Yan-Neale, Y.; Yang, G.; Lin, F.; Yin, H.; Gao, H.; Kipp, D. R.; Zhao, S.; McNamara, J. T.; Sprague, E. R.; Zheng, B.; Lin, Y.; Cho, Y. S.; Gu, J.; Crawford, K.; Ciccone, D.; Vitari, A. C.; Lai, A.; Capka, V.; Hurov, K.; Porter, J. A.; Tallarico, J.; Mickanin, C.; Lees, E.; Pagliarini, R.; Keen, N.; Schmelzle, T.; Hofmann, F.; Stegmeier, F.; Sellers, W. R.; et al. *Science* **2016**, *351*, 1208−1213.

(11) Kryukov, G. V.; Wilson, F. H.; Ruth, J. R.; Paulk, J.; Tsherniak, A.; Marlow, S. E.; Vazquez, F.; Weir, B. A.; Fitzgerald, M. E.; Tanaka, M.; Bielski, C. M.; Scott, J. M.; Dennis, C.; Cowley, G. S.; Boehm, J. S.; Root, D. E.; Golub, T. R.; Clish, C. B.; Bradner, J. E.; Hahn, W. C.; Garraway, L. A. *Science* **2016**, *351*, 1214−1218.

(12) Basu, I.; Cordovano, G.; Das, I.; Belbin, T. J.; Guha, C.; Schramm, V. L. *J. Biol. Chem.* **2007**, *282*, 21477−21486.

(13) Basu, I.; Locker, J.; Cassera, M. B.; Belbin, T. J.; Merino, E. F.; Dong, X.; Schramm, V. L.; et al. *J. Biol. Chem.* **2011**, *286*, 4902−4911.

(14) Fuqua, W. C.; Winans, S. C.; Greenberg, E. P. *J. Bacteriol.* **1994**, *176*, 269−275.

(15) Schramm, V. L.; Gutierrez, J. A.; Cordovano, G.; Basu, I.; Guha, C.; Belbin, T. J.; Evans, G. B.; Tyler, P. C.; Furneaux, R. H. *Nucleic Acids Symp. Ser. (Oxf).* **2008**, *52*, 75−76.

(16) Gutierrez, J. A.; Crowder, T.; Rinaldo-Matthis, A.; Ho, M. C.; Almo, S. C.; Schramm, V. L. *Nat. Chem. Biol.* **2009**, *5*, 251−257.

(17) Dairi, T. *J. Antibiot.* **2009**, *62*, 347−352.

(18) Li, X.; Apel, D.; Gaynor, E. C.; Tanner, M. E. *J. Biol. Chem.* **2011**, *286*, 19392−19398.

(19) Wang, S.; Haapalainen, A. M.; Yan, F.; Du, Q.; Tyler, P. C.; Evans, G. B.; Rinaldo-Matthis, A.; Brown, R. L.; Norris, G. E.; Almo, S. C.; Schramm, V. L. *Biochemistry* **2012**, *51*, 6892−6894.

(20) Wang, S.; Cameron, S. A.; Clinch, K.; Evans, G. B.; Wu, Z.; Schramm, V. L.; Tyler, P. C. *J. Am. Chem. Soc.* **2015**, *137*, 14275−14280.

(21) Evans, G. B.; Furneaux, R. H.; Schramm, V. L.; Singh, V.; Tyler, P. C. *J. Med. Chem.* **2004**, *47*, 3275−3281.

(22) Evans, G. B.; Furneaux, R. H.; Lenz, D. H.; Painter, G. F.; Schramm, V. L.; Singh, V.; Tyler, P. C. *J. Med. Chem.* **2005**, *48*, 4679−4689.

(23) Guan, R.; Ho, M. C.; Brenowitz, M.; Tyler, P. C.; Evans, G. B.; Almo, S. C.; Schramm, V. L. *Biochemistry* **2011**, *50*, 10408−10417.

(24) Burgos, E. S.; Gulab, S. A.; Cassera, M. B.; Schramm, V. L. *Anal. Chem.* **2012**, *84*, 3593−3598.

(25) Parkin, D. W.; Leung, H. B.; Schramm, V. L. *J. Biol. Chem.* **1984**, *259*, 9411−9417.

(26) Ishikura, Y.; Kanazawa, T.; Sato, T. *Bull. Chem. Soc. Jpn.* **1962**, *35*, 731−735.

(27) Montgomery, J. A.; Shortnacy, A. T.; Thomas, H. J. *J. Med. Chem.* **1974**, *17*, 1197−1207.

(28) Thomas, K.; Haapalainen, A. M.; Burgos, E. S.; Evans, G. B.; Tyler, P. C.; Gulab, S.; Guan, R.; Schramm, V. L. *Biochemistry* **2012**, *51*, 7541−7550.

(29) Singh, V.; Schramm, V. L. *J. Am. Chem. Soc.* **2006**, *128*, 14691−14696.

(30) Morrison, J. F. *Biochim. Biophys. Acta* **1969**, *185*, 269−286.

(31) Porter, D. J. *J. Biol. Chem.* **1992**, *267*, 7342−7351.

(32) Ghanem, M.; Saen-oon, S.; Zhadin, N.; Wing, C.; Cahill, S. M.; Schwartz, S. D.; Callender, R.; Schramm, V. L. *Biochemistry* **2008**, *47*, 3202−3215.

(33) Appleby, T. C.; Erion, M. D.; Ealick, S. E. *Structure* **1999**, *7*, 629−641.

(34) Singh, V.; Shi, W.; Evans, G. B.; Tyler, P. C.; Furneaux, R. H.; Schramm, V. L.; et al. *Biochemistry* **2004**, *43*, 9−18.

(35) Du, Q.; Wang, Z.; Schramm, V. L. *Proc. Natl. Acad. Sci. U. S. A.* **2016**, *113*, 2916−2921.

(36) Murray, B.; Antonyuk, S. V.; Marina, A.; Van Liempd, S. M.; Lu, S. C.; Mato, J. M.; Hasnain, S. S.; Rojas, A. L. *IUCrJ* **2014**, *1*, 240−249.

(37) Otwinowski, Z.; Minor, W. *Methods Enzymol.* **1997**, *276*, 307−326.

(38) Vagin, A.; Teplyakov, A. *J. Appl. Crystallogr.* **1997**, *30*, 1022−1025.

(39) Murshudov, G. N.; Skubák, P.; Lebedev, A. A.; Pannu, N. S.; Steiner, R. A.; Nicholls, R. S.; Winn, M. D.; Long, F.; Vagin, A. A. *Acta Crystallogr., Sect. D: Biol. Crystallogr.* **2011**, *67*, 355−367.

(40) Emsley, P.; Lohkamp, B.; Scott, W. G.; Cowtan, K. *Acta Crystallogr., Sect. D: Biol. Crystallogr.* **2010**, *66*, 486−501.

(41) Lebedev, A. A.; Young, P.; Isupov, M. N.; Moroz, O. V.; Vagin, A. A.; Murshudov, G. N. *Acta Crystallogr., Sect. D: Biol. Crystallogr.* **2012**, *68*, 431−440.

(42) Shi, W.; Tanaka, K. S. E.; Crother, T. R.; Taylor, M. W.; Almo, S. C.; Schramm, V. L. *Biochemistry* **2001**, *40*, 10800−10809.

DOI: 10.1021/acs.analchem.6b03621
Anal. Chem. XXXX, XXX, XXX−XXX